Supplementary Information

Elastoviscoplasticity, Hyperaging, and Time–Age-Time–Temperature Superposition in Aqueous Dispersions of Bentonite Clay

Joshua David John Rathinaraj[a], Kyle R. Lennon[b], Miguel Gonzalez[c], Ashok Santra[c], James W. Swan[b], and Gareth H. McKinley[a]

a) Department of Mechanical Engineering, Massachusetts Institute of Technology, Cambridge, MA, USA.

b) Department of Chemical Engineering, Massachusetts Institute of Technology, Cambridge, MA, USA.

c) Aramco Services Company: Aramco Research Center, Houston, TX, USA.

1. Material information:

The Sodium bentonite powder used in this work comprises montmorillonite clay, with the chemical formula $Na_{0.33}[(Al_{1.67}Mg_{0.33})(O(OH))_2(SiO_2)_4]$, and the quartz mineral SiO_2. An X-ray diffraction (XRD) spectrum for the dry clay powder is shown in Figure S1. The size of these anhydrous clay particles range from 20 μm to 200 μm. The 50th percentile particle diameter of the clay particles is $D_{50} = 65\ \mu m$, which was inferred from the cumulative distribution function of particle sizes shown in Figure S2(a). From the cumulative particle size distribution, we also infer the distribution of volume among particles of a given size, which is presented in Figure S2(b). In Figure S2, the 'size' measure for the particles is chosen to be the diameter.

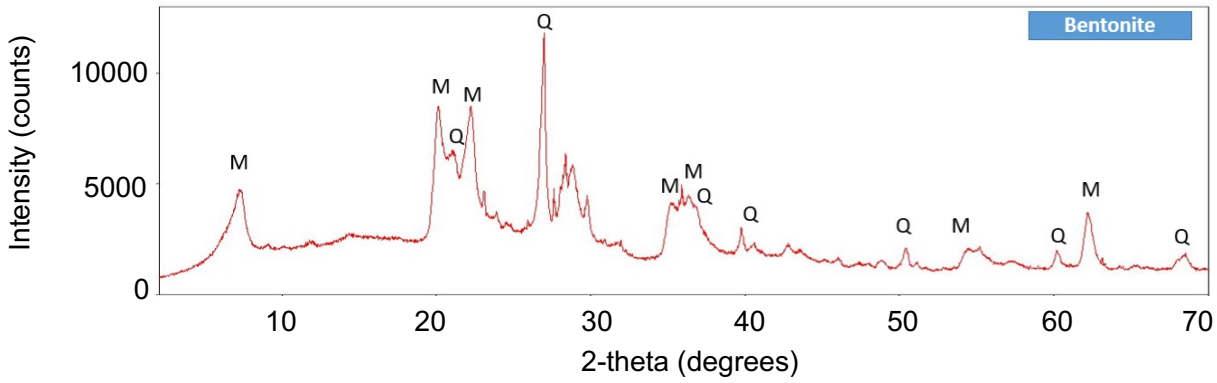

Figure S1: The XRD analysis of the Wyoming bentonite clay powder used in this work, indicating the presence of montmorillonite and quartz. The letter 'M' denotes features associated with montmorillonite, and the letter 'Q' denotes features associated with quartz.

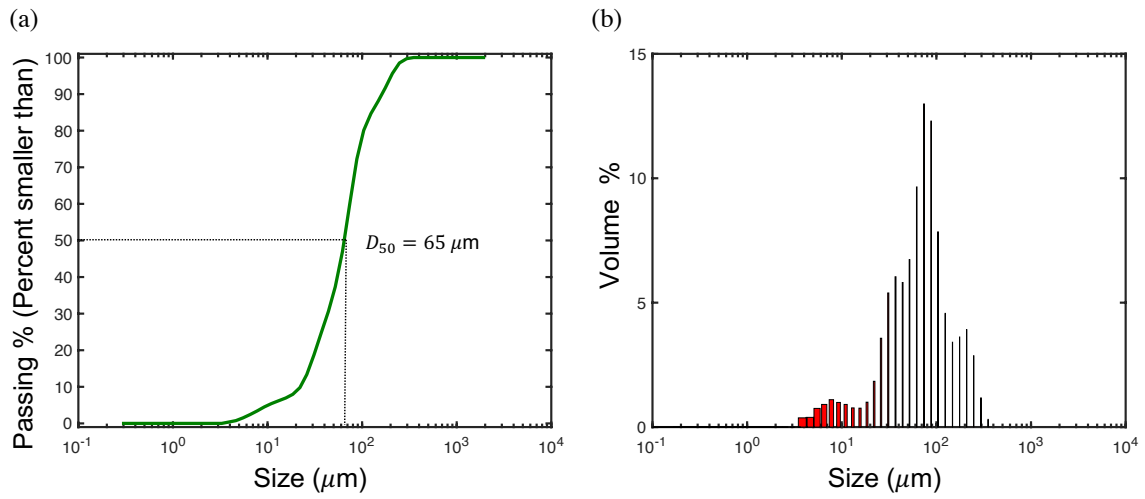

Figure S2: Particle size distributions of the anhydrous bentonite particles. (a) Cumulative distribution function of the particle size, referred to as the 'Passing %', or the percentage of particles with size smaller than the corresponding size value (μm) given on the abscissa. The D_{50} (50th percentile particle diameter) of the anhydrous bentonite particles is 65 μm. (b) The 'Volume %', or the percent of the total particle volume associated with particles of a given size, for the Wyoming anhydrous bentonite particles.

2. Flow curve:

The steady shear flow curves obtained at different temperatures and different age times via an increasing flow sweep and a decreasing flow sweep were fit to the Herschel-Bulkley model:

$$\sigma = \sigma_y + k\,\dot{\gamma}^n.$$

These Herschel-Bulkley fits are shown in Figure S3 and help to quantify the increase in the dynamic yield stress with increasing temperature and age times. The model parameters that minimize the mean-squared error between model predictions and data are tabulated below:

Temp [˚C]	$\sigma_y\ [Pa]$		$k\ [Pa \cdot s^n]$		n	
	t: $180 - 1980\ s$ Up	t: $2100 - 3900\ s$ Down	t: $180 - 1980\ s$ Up	t: $2100 - 3900\ s$ Down	t: $180 - 1980\ s$ Up	t: $2100 - 3900\ s$ Down
10	2.5	3.1	0.66	0.55	0.52	0.54
25	3.0	4.1	0.64	0.34	0.49	0.59
49	5.0	8.1	0.73	0.026	0.44	1
65	7.6	10.2	0.17	0.015	0.64	1

From the tabulated values and Figure S3, we see that the yield stress increases with age time and with temperature.

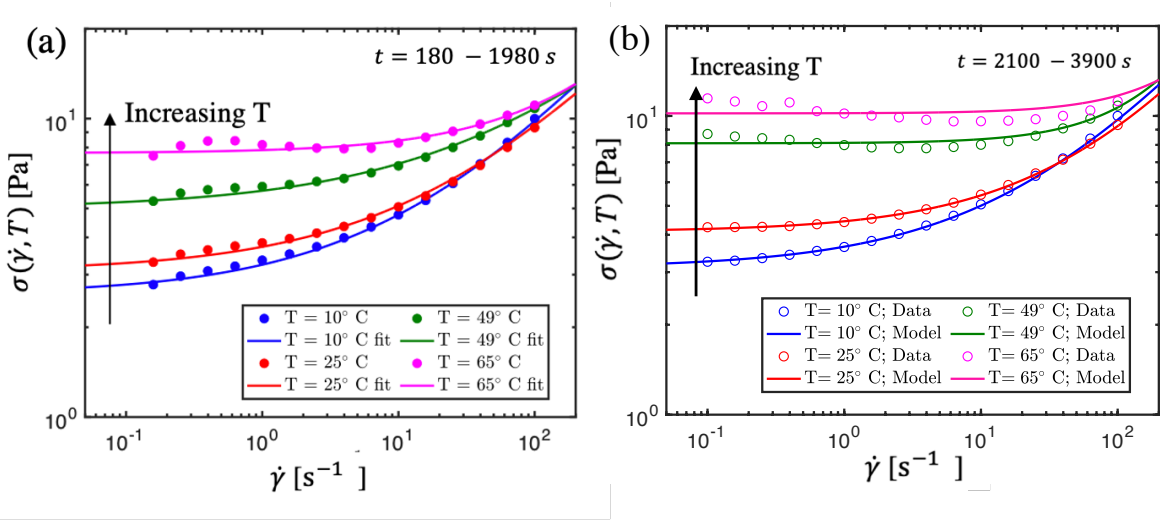

Figure S3: (a) Flow curves measured at different temperatures via increasing-rate sweeps ($t = 180 - 1980\ s$). (b) Flow curves measured at different temperatures via decreasing-rate sweeps $t = 2100 - 3900\ s$). The Herschel Bulkley (HB) model is fit to the data in both (a) and (b) to calculate the apparent static yield stress.

3. Step relaxation after step strain:

The relaxation modulus at temperatures T = 25˚C, 37˚C, and 49˚C was measured via stress relaxation experiments with a step strain of $\gamma_0 = 0.02$, applied at various wait times $t_w \in$ [45, 400] s, as shown in Figure S4. The stress relaxation experiments at different temperatures share the characteristic that the relaxation modulus increases with t_w. This increase is attributed to the stronger, more developed microstructure in dispersions that have undergone more aging, compared to the relatively weak character of the microstructure in the young dispersions. In other words, with time the discotic clay particles have rearranged themselves to reduce the free energy of the bentonite clay system. The relaxation modulus also decays faster for small wait times, corresponding to a progressive slowing of relaxation dynamics with rheological aging as the system gradually settles into a more energetically favorable microstructural state.

For each temperature, the stress relaxation data measured in laboratory time are transformed to the material time domain following the procedures outlined in Section 5.1 of the main text, and subsequently collapsed onto time—age-time master curves via vertical shifting. We fit these master curves to the fractional Maxwell gel constitutive equation with constant relaxation dynamics in the material time domain, as described in Section 5.2 of the main text. The model fits to the data in the material time domain are depicted in Figure S5(a), (c), and (e) for temperatures T = 25˚C, 37˚C, and 49˚C, respectively. The fractional Maxwell constitutive equation in the material time domain is then transformed back to the laboratory time domain

using eq.(19) and eq. (20) in the main text, which captures the non-ergodic aging phenomena. The resulting model predictions in the laboratory time are also in good agreement with the data, as shown in Figure S5(b), (d) and (f) for temperatures T = 25˚C, 37˚C, and 49˚C, respectively.

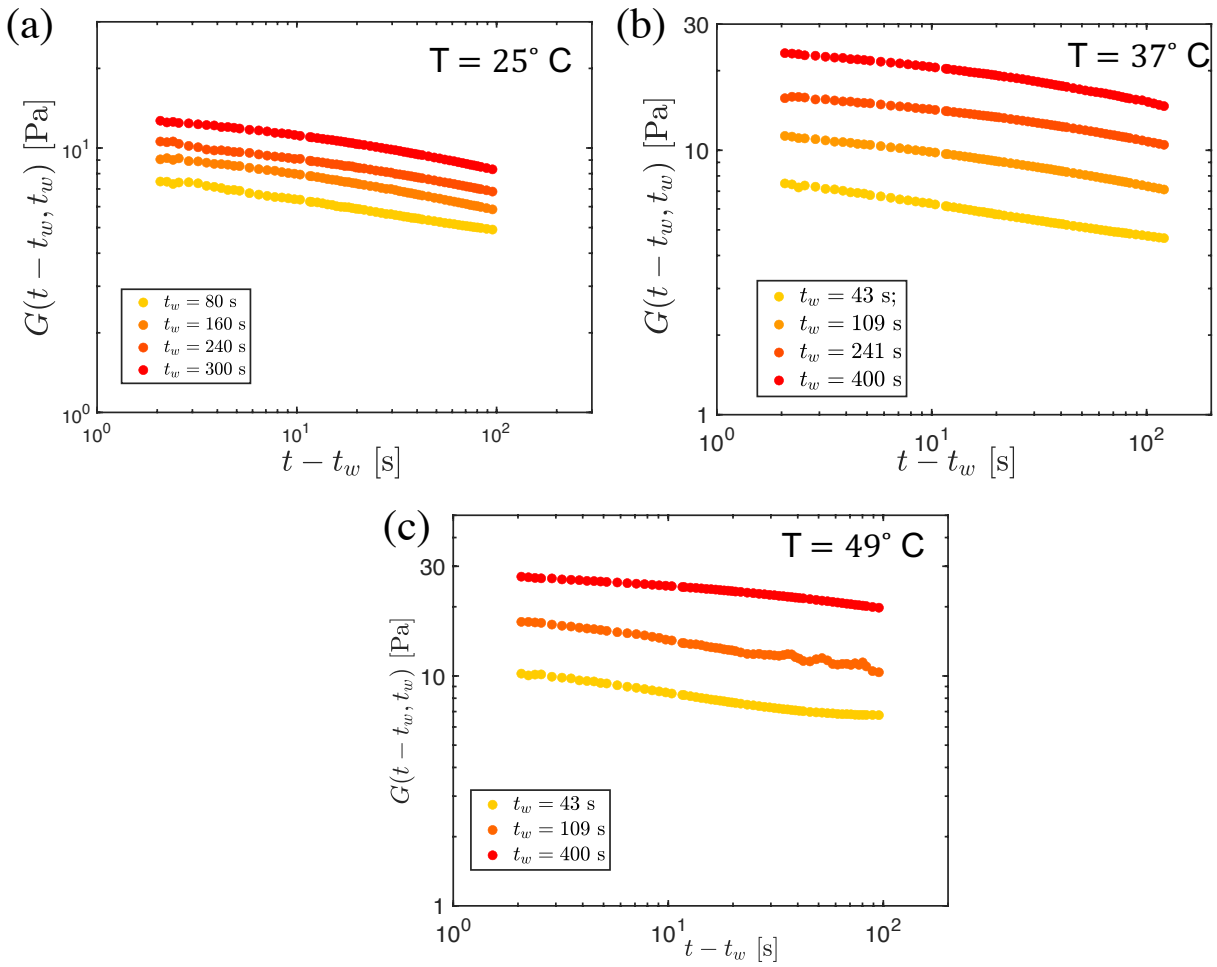

Figure S4: The measured relaxation modulus in the laboratory time frame for different wait times at T = 25˚C, T = 37˚C, and T = 49˚C are shown in (a), (b) and (c), respectively. The relaxation modulus and relaxation time both increase with the age of the dispersion at all temperatures. The step strain amplitude imposed for all experiments is $\gamma_0 = 0.02$.

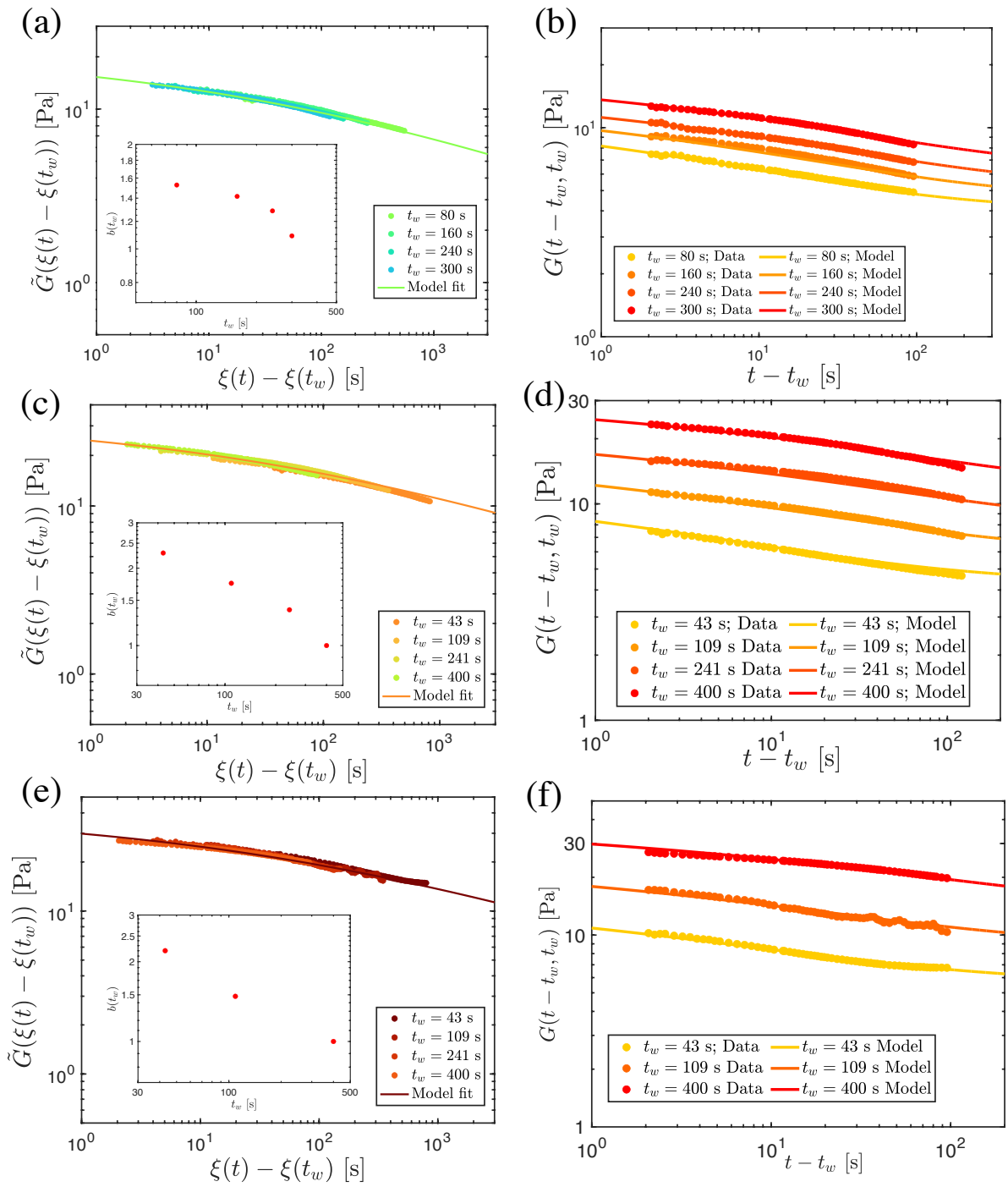

Figure S5: The relaxation modulus as a function of material time is shown in (a), (c), (e) for T = 25˚, 37˚C, 49˚C, respectively, along with the corresponding relaxation modulus data as a function of laboratory time in (b), (d), (f). The experimental data (symbols) and predictions of the fractional Maxwell gel model (lines) in (a), (c) and (e) are those from (b), (d) and (f) transformed to material time using the parameters $\mu = 1.45, 1.32,$ and 1.20, respectively, with a reference time of $t_R = 400$ s and the respective vertical shift factors $b(t_w)$ (shown in inset of (a), (c) and (e)).